Mon. Not. R. Astron. Soc. **373,** 993–1003 (2006) doi:10.1111/j.1365-2966.2006.11044.x

The search for the origin of the Local Bubble redivivus

B. Fuchs,[1⋆] D. Breitschwerdt,[2] M. A. de Avillez,[2,3] C. Dettbarn[1] and C. Flynn[4]

[1]*Astronomisches Rechen-Institut, ZAH, Mönchhofstraße 12-14, D-69120 Heidelberg, Germany*
[2]*Institut für Astronomie der Universität Wien, Türkenschanzstraße 17, A-1180 Wien, Austria*
[3]*Department of Mathematics, University of Évora, R. Romão Ramalho 59, 7000 Évora, Portugal*
[4]*Tuorla Observatory, University of Turku, Väisäläntie 20, FI-21500 Piikkiö, Finland*

Accepted 2006 September 7. Received 2006 September 7; in original form 2006 April 26

ABSTRACT

We present a new unbiased search and analysis of all B stars in the solar neighbourhood (within a volume of 400 pc diameter) using the Arivel data base to track down the remains of the OB associations, which hosted the supernovae (SNe) responsible for the Local Bubble (LB) in the interstellar gas. We find after careful dereddening and by comparison with theoretical isochrones, that besides the Upper Scorpius the Upper Centaurus Lupus and Lower Centaurus Crux subgroups are the youngest stellar associations in the solar neighbourhood with ages of 20–30 Myr, in agreement with previous work. In search for the 'smoking gun' of the origin of the LB, we have traced the paths of the associations back into the past and found that they entered the present bubble region 10–15 Myr ago. We argue that the LB began to form then and estimate that 14–20 SNe have gone off since. It is shown that the implied energy input is sufficient to excavate a bubble of the presently observed size.

Key words: open clusters and associations: individual: Sco OB2 – solar neighbourhood – ISM: individual: local bubble.

1 INTRODUCTION

The Local Bubble (LB), a low-density X-ray emitting cavity deficient of H I, is our Galactic habitat. Yet, until recently, its origin remained mysterious. It was conjectured to be the result of one or several supernova (SN) explosions (e.g. Cox & Anderson 1982; Innes & Hartquist 1984; Smith & Cox 2001), but firm evidence was lacking, as no OB association was found within its boundaries, extending about 200 pc in the Galactic plane, and 600 pc perpendicular to it, but inclined by about 20° with respect to the axis of Galactic rotation, similar to Gould's Belt (cf. Lallement et al. 2003). Further problems arose, since the X-ray and EUV spectra measured in the Wisconsin Survey, by *ROSAT* PSPC, DXS, XQC and EUVE were severely at odds with a thermal hot plasma in collisional ionization equilibrium (CIE) as was pointed out by Jelinsky, Vallerga & Edelstein (1995), Sanders et al. (2001) and McCammon et al. (2002). Most recently Hurwitz, Sasseen & Sirk (2005) analysed CHIPS data and found an extremely low emissivity of EUV iron lines. The underabundance of soft X-ray lines can be naturally explained if the plasma is in a state of delayed recombination (Breitschwerdt & Schmutzler 1994; Breitschwerdt 2001), but a high-resolution numerical hydrodynamical evolution model is needed to better constrain non-equilibrium models. Spectral discrepancies between models and observations can be alleviated if there is a substantial contribution from very local sources, such as the Earth's exosphere (Freyberg 1998) or charge exchange reactions between solar wind ions (SWCE) and heliospheric gas (Lallement 2004). At present it is unclear what fraction can be attributed to these very nearby sources, although there is fairly robust evidence that even in the extreme case of all of the X-ray emission being due to SWCE in a certain direction, a substantial LB fraction remains, especially perpendicular to the disc. For further details on LB properties we refer to the review of Breitschwerdt (2001) and the conference proceedings *The Local Bubble and Beyond* (Breitschwerdt, Freyberg & Trümper 1998).

All these shortcomings have led several authors to speculate that if the LB is not a classical superbubble, but rather an appendix of the neighbouring Loop I superbubble, which was expanding into an interarm region between the Sagittarius and the Perseus spiral arms of the Galaxy (Bochkarev 1987; Frisch 1995). However, the existence of a 'wall' between the two bubbles, showing up in absorption of soft X-rays in *ROSAT* PSPC images (Egger & Aschenbach 1995) renders this scenario not very plausible.

The search for the 'smoking gun' of the origin of the LB proved partially successful by discovering that moving groups of young stars in the solar neighbourhood could provide an adequate number of SN explosions while crossing the path of the LB. Berghöfer & Breitschwerdt (2002, hereafter BB02) calculated the trajectory of the Pleiades subgroup B1 backwards in time, and found that 19 SNe could have exploded between 10–20 Myr ago in the region that is occupied by the LB. The remaining stars of B1 are now part of the Scorpius Centaurus OB association. It could be shown that this is in good agreement with the size of the LB and the present soft X-ray emissivity. A similar analysis was carried out by Maíz-Apellániz

⋆E-mail: fuchs@ari.uni-heidelberg.de

(2001), who calculated backwards in time the trajectories of Sco Cen subgroups and claimed that about six SNe that went off in the Lower Centaurus Crux (LCC) subgroup of the Sco OB2 association 7–9 Myr ago formed the LB.

While these analyses represent a major step towards the understanding of the origin of the LB they are not free from bias, in particular the assumption that *certain stellar groups should* be responsible for the sought SN explosions. The purpose of this paper is to scrutinize *all stars* that are within a volume of about 400 pc in diameter centred around the Sun, and to perform a selection according to spectral and kinematical properties. The latter is based on 3D space velocities of the stars. Thus our approach is complementary to studies like by de Zeeuw et al. (1999) which are based on proper motions alone. Sartori, Lépine & Dias (2003) do include radial velocities when analysing the subgroups of the Sco OB2 association, but work from a list of stars pre-selected by de Zeeuw et al. (1999). From their position in the HR diagram and the turn-off point from the zero-age main-sequence, we can reliably determine the age of the stars and estimate the number of SNe within a defined region, such as the LB.

The paper is organized as follows. In the next section we describe our search strategy for the remnants of the OB association responsible for the origin of the LB. In Section 3 we discuss the consistency of our findings with the properties of the LB as observed today, and present a high-resolution 3D hydrodynamical simulation of the formation of the LB in the local interstellar gas. In the final section we summarize our conclusions.

2 SEARCH FOR NEARBY OB ASSOCIATIONS

Even though the Sco OB2 association has been claimed with good reason to be responsible for the origin of the LB (Maíz-Apellániz 2001; BB02), a fresh, unprejudiced search for the OB association, that might have triggered the formation of the LB, will improve and harmonize previous studies. As starting point we used the *Hipparcos* catalogue (ESA 1997) from which we selected all stars bluer than $(B-V) < -0.05$ with parallaxes larger than 5 mas, because otherwise the distances would be too inaccurate. Drimmel, Smart & Lattanzi (2000) find by a comparison with the Tycho catalogue that the *Hipparcos* catalogue is about 97 per cent complete down to $V = 7.5$ which corresponds at a distance of $1/(5\,\mathrm{mas}) = 200$ pc to an absolute magnitude of $M_V = 1$. Allowing for an extinction of $A_V \leqslant 0.2$ we have $M_V < 1.2$, and we have chosen the colour cut in $(B-V)$ accordingly. We have obtained this way an unbiased complete sample of 762 B stars within a distance of 200 pc from the Sun. One of the bluest stars is the B0.5 star α Cru. The stars of the sample show at this stage already a well-defined main sequence in the colour–magnitude diagram. There are a few stars lying several magnitudes below the main sequence, which are probably subdwarfs. We have omitted these, $M_V > 3.0$ mag, because we are interested in young stars. All stars in our list appear in the Arivel data base, which combines *Hipparcos* parallaxes and proper motions with radial velocity data collected from the literature (Dettborn et al., in preparation). We find that for 610 stars radial velocities are available. These are accurate enough to be used for a kinematical analysis. We have tested if the availability of radial velocities is correlated with the colours of the stars and find that the 152 out of 762 stars for which no radial velocity is known lie above $(B-V) > -0.1$. We discuss the implications of this effect on the determination of the expected number of SNe below. For each star spatial X, Y and Z coordinates and the corresponding U, V and W velocity components have been calculated. The coordinates shown in Fig. 1 are centred on the Sun with X-axis pointing towards $l = 0^\circ$, $b = 0^\circ$, Y-axis towards $l = 90^\circ$, $b = 0^\circ$ and Z-axis towards $b = 90^\circ$, respectively. Since OB associations disperse slowly on time-scales of the order of several 10^7 yr (Blaauw 1964), we have searched for kinematically coherent structures in our sample. For this purpose we have traced the positions of the stars backward in time over 3×10^7 yr. Stellar orbits have been calculated using the epicyclic equations of motion for the stars in the sample (Lindblad 1959; Wielen 1982)

$$
\begin{aligned}
X(t) &= X(0) - \frac{V(0)}{-2B}[1-\cos(\kappa t)] + \frac{U(0)}{\kappa}\sin(\kappa t),\\
U(t) &= U(0)\cos(\kappa t) - \frac{\kappa}{-2B}V(0)\sin(\kappa t),\\
Y(t) &= Y(0) + 2A\left[X(0) - \frac{V(0)}{-2B}\right]t\\
&\quad + \frac{\Omega_0}{-B\kappa}V(0)\sin(\kappa t) + \frac{2\Omega_0}{\kappa^2}U(0)[1-\cos(\kappa t)],\\
V(t) &= \frac{-2B}{\kappa}U(0)\sin(\kappa t) + V(0)\cos(\kappa t),\\
Z(t) &= \frac{W(0)}{\nu}\sin(\nu t) + Z(0)\cos(\nu t),\\
W(t) &= W(0)\cos(\nu t) - Z(0)\nu\sin(\nu t). \qquad (1)
\end{aligned}
$$

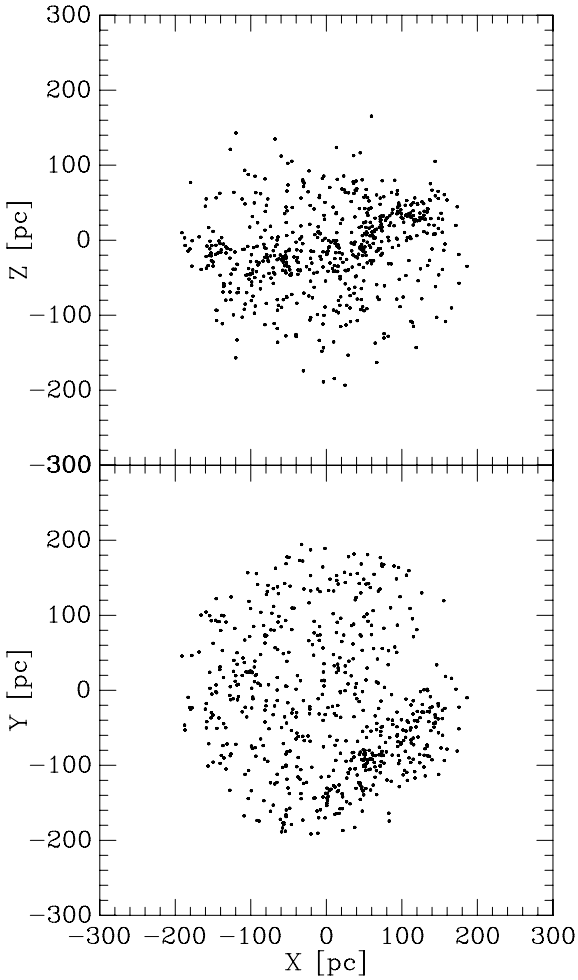

Figure 1. Positions of 610 stars drawn from the *Hipparcos* catalogue. The selected stars have colours $B-V < -0.05$ and for each star its radial velocity is known. The X-axis points towards the Galactic Centre, Y-axis into the direction of Galactic rotation and Z-axis towards the North Galactic Pole, respectively.

In equations (1) κ denotes the epicyclic frequency, $\kappa = \sqrt{-4\Omega_0 B}$. A and B are the Oort constants, and Ω_0 is the angular frequency of the rotation of the local standard of rest around the Galactic Centre, $\Omega_0 = V_{\rm LSR}/{\rm R}_\odot$. ν denotes the vertical oscillation frequency which is related to the local density ρ_0 by the Poisson equation as $\nu = \sqrt{4\pi G \rho_0}$, where G is the constant of gravitation. For the angular velocity of the local standard of rest we have adopted a value of $\Omega_0 = 220$ km s^{-1}/8 kpc. The choice of the Oort constants was guided by the consideration that they describe in equations (1) the smooth Galactic gravitational potential. The latter is consistent with an essentially flat shape of the local Galactic rotation curve, $A = -B = \Omega_0/2$ (Feast & Whitelock 1997). This must not be confused with determinations of A and B using OB stars as, for instance, in the studies of Torra, Fernández & Figueras (2000) or Elias, Alfaro & Cabrera-Caño (2006). These reflect peculiarities of the orbits of the OB stars in Gould's Belt related to the velocities with which they were born, but not the characteristic smooth shape of the Galactic potential. For the local density we adopt a value of $\rho_0 = 0.1\,\mathcal{M}_\odot\,{\rm pc}^{-3}$ (Holmberg & Flynn 2004). These parameter values imply $\kappa = 0.039\,{\rm km\,s^{-1}\,pc^{-1}} = 4 \times 10^{-8}\,{\rm yr^{-1}}$ and $\nu = 0.074\,{\rm km\,s^{-1}\,pc^{-1}} = 7.5 \times 10^{-8}\,{\rm yr^{-1}}$. In Fig. 2 we show the positions of the stars today and 3×10^7 yr ago. Apparently most stars came from directions $-90^\circ < l < 90^\circ$ and stayed close to the Galactic mid-plane. Most of the 610 stars do not belong to the OB association, which hosted the SNe responsible for the origin of the LB, and have space velocities different from the velocity of the association. Thus they are dispersed away into a wide cloud. However, the overdense regions in Fig. 2 indicate that there is a considerable number of stars which stayed together. The larger size of the overdense regions in the back projected sample compared to its size today is obviously due to the observational errors. The typical accuracy of *Hipparcos* proper motions is about 1 mas yr^{-1} which corresponds at a distance of 100 pc to a velocity of 0.5 km s^{-1}, whereas the accuracy of the radial velocities is several km s^{-1}. Taken together with an expansion velocity of the order of 10 km s^{-1} (Blaauw 1964), this implies a spreading of the overdensity, which represents the kinematically homogenous group of stars, to a size of roughly 500×500 pc in X and Y. As can be seen from Fig. 2 there is an outer shroud of stars which lies at greater distances from the core of the overdensity. These must be stars with genuinely different space velocities from the kinematically homogenous group of stars. We identify this kinematically homogeneous group of stars as an OB association and select 302 stars lying in the windows indicated as dashed lines in Fig. 2. As expected these stars are more or less closely related to the Sco OB2 association.

In Fig. 3 we show the present-day velocity distribution of the 302 selected stars. Since the velocity dispersion of an OB association is of the order of 10 km s^{-1} (Blaauw 1964) or even less (Kamaya 2004), we make a second selection indicated by windows drawn as dashed lines in Fig. 3. This leaves a sample of 236 stars which we analyse in the following. *Hipparcos* numbers of these stars are listed in Appendix A.

The final sample is shown as a colour–magnitude diagram in Fig. 4. For this purpose we have cross-identified the sample stars in the Geneva photometry data base (Mermilliod, Hauck & Mermilliod 1997) and replaced the $(B-V)_T$ colours given in the *Hipparcos* catalogue by $(B-V)_J$ colours, because they can be then directly compared with theoretical isochrones available in the literature. In the colour range, which we consider here, $B-V$ given in the Tycho system cannot be transformed directly to the Johnson system (ESA 1997). The absolute magnitudes have been determined from the visual magnitudes given in the *Hipparcos* catalogue in the Johnson system.

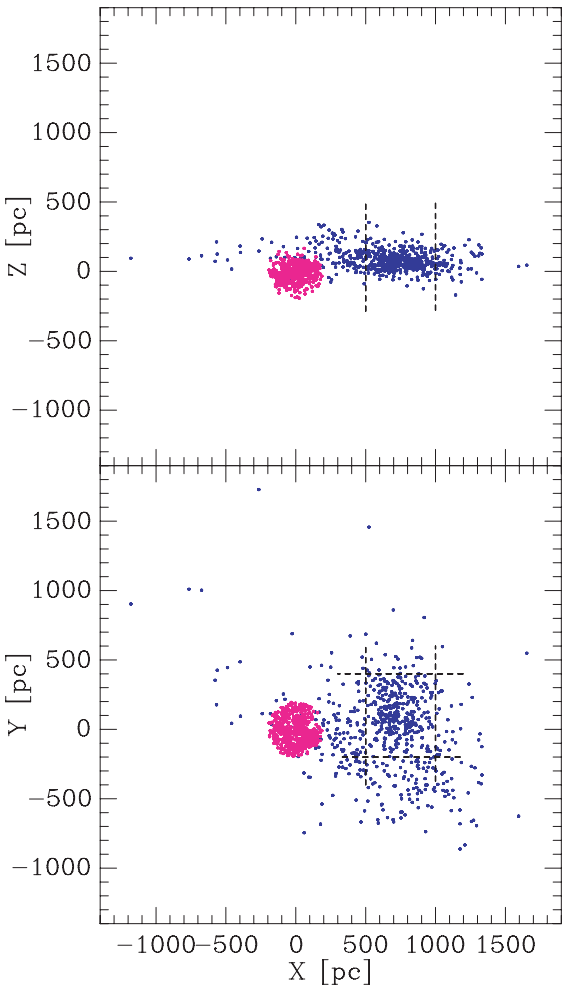

Figure 2. Positions of the originally selected stars today (pink) and 3×10^7 yr ago (blue). The Sun is at rest in the diagrams. Stars lying in the windows indicated by dashed lines are identified as putative members of the searched for OB association.

We have compared our sample with the extensive membership list of the Sco OB2 association compiled by de Zeeuw et al. (1999) who applied a combination of a modified convergent point method and the so-called spaghetti method (Hoogerwerf & Aguilar 1999) to *Hipparcos* data. Of particular interest are the membership lists of the subgroups Upper Scorpius (US), Upper Centaurus Lupus (UCL) and LCC. With only very few exceptions all stars in the membership lists, which fulfil our colour selection criterion, appear also in our sample, which gives confidence in our selection procedure. A few stars from our final sample could be identified additionally in the membership list of de Geus, de Zeeuw & Lub (1989) as members of the subgroups. The 79 stars common to both lists are colour coded in Fig. 4 and listed separately in Appendix A.

3 RESULTS AND DISCUSSION

3.1 The search for the 'smoking gun'

The colour–magnitude diagram presented in Fig. 4 shows a clearly discernible main sequence, which is particularly well delineated by

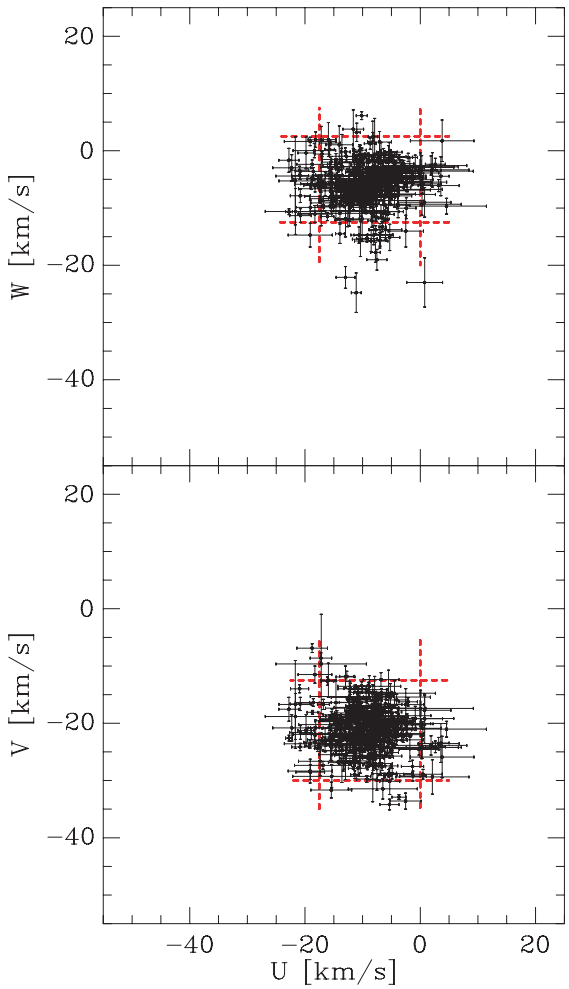

Figure 3. Present-day velocity distribution of the 302 selected stars. A second selection is made of the stars lying in the windows indicated by dashed lines.

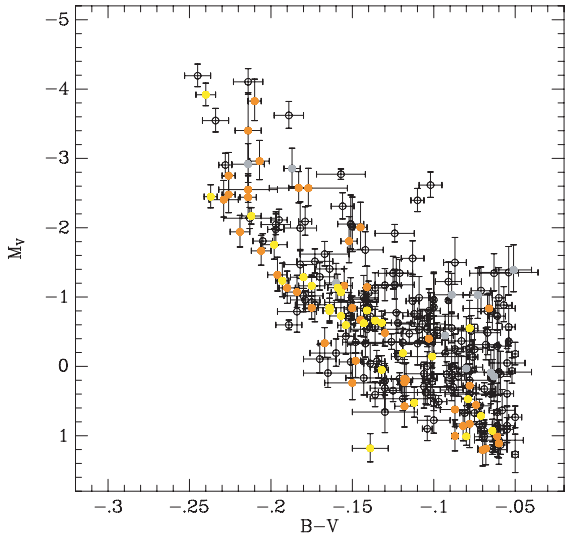

Figure 4. Colour–magnitude diagram of the final sample (236 stars). Members of the UCL subgroup of Sco OB2 are highlighted in orange, LCC in yellow and US in grey, respectively.

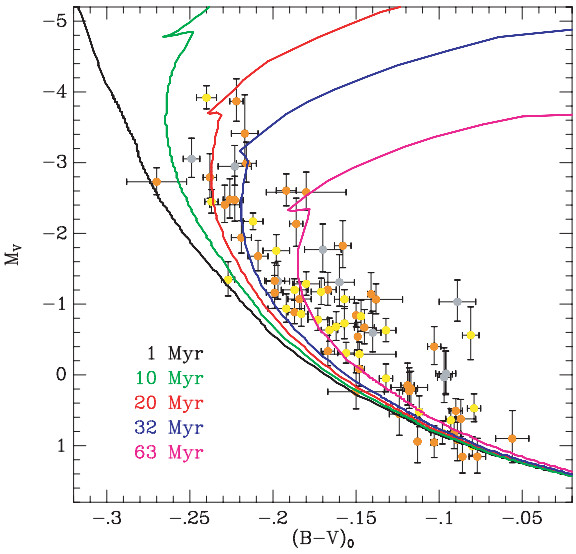

Figure 5. Dereddened colour–magnitude diagram of the members of the US (grey), UCL (orange) and LCC (yellow) subgroups. The solid lines are theoretical isochrones colour coded according to their ages.

the members of the UCL group. The turn-off point at the tip is defined by both the members of the UCL and the LCC subgroups. Apparently these are together with the US subgroup indeed the youngest OB associations in the solar neighbourhood (de Geus et al. 1989; Sartori et al. 2003). In order to determine their age we have compared the colour–magnitude diagram with theoretical isochrones calculated by Schaller et al. (1992) for solar metallicities. Fortunately de Bruijne et al. (1999) and Sartori et al. (2003) have determined individually for most members of the US, UCL and LCC subgroups, respectively, the extinction and colour excess by comparing the observed $(V - I)_C$ colours with the intrinsic colours of stars of the same spectral type and luminosity class. Dereddened data of the 79 stars are shown together with isochrones in Fig. 5. We conclude from Fig. 5 that the ages of the UCL and LCC subgroups lie in the range of 20–30 Myr, whereas we cannot date the age of the US subgroup on the basis of our data. We note that this estimate of the ages of the subgroups is nearly twice of that of de Geus et al. (1989), who determined an age of 11–12 Myr of the LCC subgroup and 14–15 Myr of the UCL subgroup, respectively. These age estimates were revised by Sartori et al. (2003) to 16–20 Myr on the basis of the Padova isochrones (Bertelli et al. 1994) instead of the Maeder (1981a,b,c) isochrones, which were used by de Geus et al. (1989). The Schaller et al. (1992) isochrones, which we used, are an upgrade of Maeder's isochrones by the Geneva group. Moreover, we note that Sartori et al. (2003) have adopted for the majority of their stars the spectral types given in the *Hipparcos* catalogue, which might not be as reliable as the Geneva photometric data which we used. Given these uncertainties we conclude that our age datings of the LCC and UCL subgroups are consistent with the result of Sartori et al. (2003). This agrees also well with the age of Pleiades subgroup B1, which was suggested to be responsible for the origin of the LB by BB02, but is significantly larger than assumed by Maíz-Apellániz (2001), especially for the LCC subgroup. Moreover, we have examined with the help of the Simbad data base each star of the subgroups lying not on the main sequence and found that practically all these stars are either binaries or peculiar in the sense that they are variable, emission-line stars, etc. (cf. the notes to the tables), so

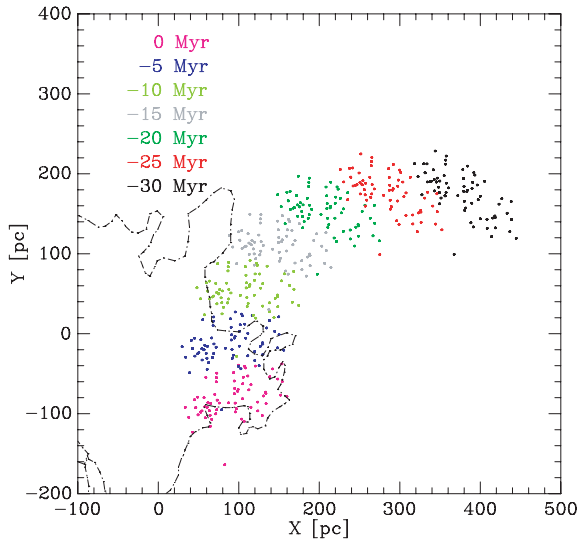

Figure 6. Path of the UCL and LCC associations over the last 30 Myr projected on to the Galactic plane. The look-back time is colour coded. The orbits are calculated backwards in the reference frame of the local standard of rest assuming for each star the same mass-weighted mean velocity of the stars. The position of the LB is indicated by the dash–dotted contour line and is at rest in this reference frame.

that their position off the main sequence in the colour–magnitude diagram shown in Fig. 5 can be explained in our interpretation by such effects.

In Fig. 6 we trace back the positions of the UCL and LCC subgroup members over the last 30 Myr using again the epicycle equations (1). However, we have not used the individual space velocities of the stars, but adopted for each star the mass-weighted mean velocity of the combined subgroups. This avoids any unphysical spread of the spatial distribution of the stars at earlier times due to the errors of the space velocity components of the stars. The stellar masses have been determined with the mass-to-magnitude relation

$$\mathcal{M}_*/\mathcal{M}_\odot = 3.857 - 1.453M_V + 0.183M_V^2 + 0.069M_v^3, \qquad (2)$$

which we have derived from a fit to the isochrone data of Schaller et al. (1992). To the mean velocity of the stars we have added the solar motion $(U, V, W)_\odot = (10, 5.3, 7.2)$ km s^{-1} (Dehnen & Binney 1998), so that the orbits are calculated in the reference frame of the local standard of rest. Since interstellar gas has usually only small peculiar motions, the local interstellar gas, and with it the LB which is indicated in Fig. 6 by the contour line taken from Lallement et al. (2003), will basically corotate with the local standard of rest around the Galactic Centre. This means that the LB is at rest in the reference frame of Fig. 6. As can been seen from Fig. 6 the path of the association has aligned itself 15 Myr ago nearly parallel to the tangential Y direction, the direction of Galactic rotation. Remnants of SN explosions occurring during this period will have experienced very little shear due to the differential rotation of the Galaxy. The shear effect is described quantitatively by the term linearly proportional to time in the epicycle equation for $Y(t)$ (cf. equation 1). The coefficient $X(0) - V(0)/(-2B)$ is the mean guiding centre radius of an orbit. If the spread of these radii is small, as was the case in the last 15 Myr, the shear effect of the Galactic differential rotation is minimized. In our view this might well explain why all SNe occurring during that time have combined together to form the LB, while SN remnants formed at earlier times have drifted away (cf. Figs 6 and 7).

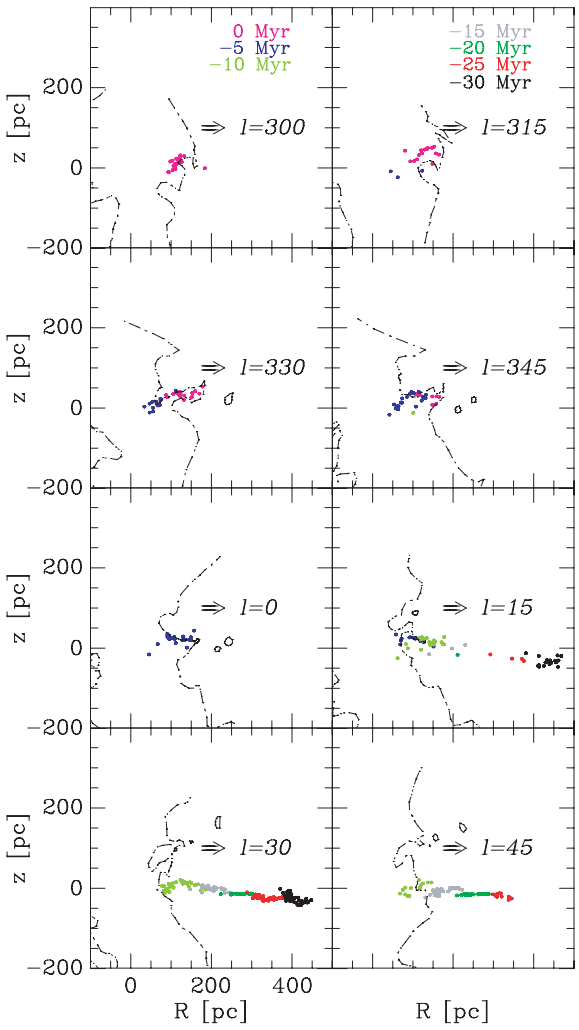

Figure 7. Meridional sections of the contours delineating the outer boundary of the LB together with the positions of the stars in the UCL and LCC associations. The horizontal axis in the upper left-hand panel points into the direction $l = 300°$, in the upper right-hand panel towards $l = 315°$ and so on. The vertical direction is always perpendicular to the Galactic mid-plane. The ages of the associations are colour coded as in Fig. 6.

Next we illustrate in Fig. 7 the position of the UCL and LCC associations relative to the LB today and at earlier times and reproduce the present-day LB contours in meridional sections through the bubble. From Fig. 6 we estimate the Galactic longitude in which direction we expect the associations to move. Choosing then the appropriate meridional section through the bubble from the paper by Lallement et al. (2003), we can determine immediately the positions of the stars in that longitude range relative to the LB. As can be seen from the upper panels of Fig. 7 the associations are today just about to exit the bubble. 5 and 10 Myr ago they were inside. The bottom right-hand panel of Fig. 7 indicates that they entered 15 Myr ago the region occupied by the LB today. In this scenario the LB was starting to form about 15 Myr ago, which is consistent with the estimates of the age of the LB by Maíz-Apellániz (2001) and BB02. In this context it should be kept in mind that although the contours determined by Lallement et al. (2003) are the presently best available, they are derived from Na I absorption-line measurements, which allow to trace the H I distribution under certain conditions,

such as low temperatures ($<10^4$ K), line saturation for high column densities, etc. (see Sfeir et al. 1999 for a discussion). In particular, the extension of the LB is *unknown* in directions where there are no background stars.

Regardless of the uncertainties of the outer boundary of the LB one might wonder, moreover, how realistic a scenario is, in which the SNe explode rather close to the edge of the present-day bubble. As our high-resolution simulation discussed in the next section shows, the location of the star cluster with respect to the centre of the bubble is not crucial. The bubble expands always fastest in the direction of the lowest ambient density and pressure. Since in the direction of the Galactic Centre the Loop I superbubble was formed almost at the same time as the LB by SNe exploding within the Sco Cen association, the pressure in this direction is very high. Hence the LB was forced to expand rather towards the anticentre direction and perpendicular to the plane, in agreement with the observations.

3.2 Unravelling the supernovae of the Local Bubble

Next we shall derive the number and masses of stars that have exploded during the journey of the OB association through the LB. Following BB02, the number of SNe, which created the LB can be estimated with the aid of the initial mass function (IMF). We have fitted an IMF of the form (Massey, Johnson & Degioia-Eastwood 1995)

$$\frac{\mathrm{d}N}{\mathrm{d}\mathcal{M}} = \left.\frac{\mathrm{d}N}{\mathrm{d}\mathcal{M}}\right|_0 \mathcal{M}^{\Gamma-1}, \tag{3}$$

with an index $\Gamma = -1.1 \pm 0.1$ to the data. Masses are given in units of solar masses. The lower end of the main sequence at $M_V = 1$ mag corresponds to A0 stars with masses of $\mathcal{M}_\mathrm{l} = 2.6\,\mathcal{M}_\odot$ and the upper tip at $M_V = -3.7$ mag to B0 stars with masses of $\mathcal{M}_\mathrm{u} = 8.2\,\mathcal{M}_\odot$ (Schaller et al. 1992), respectively. The total number of stars in the UCL and LCC associations, respectively, allow the determination of the normalization constants,

$$N = \int_{2.6}^{8.2} \left.\frac{\mathrm{d}N}{\mathrm{d}\mathcal{M}}\right|_0 \mathcal{M}^{-2.1}\mathrm{d}\mathcal{M} = 0.228 \left.\frac{\mathrm{d}N}{\mathrm{d}\mathcal{M}}\right|_0, \tag{4}$$

implying $\mathrm{d}N/\mathrm{d}\mathcal{M}|_0 = 184$ for the 42 UCL and $\mathrm{d}N/\mathrm{d}\mathcal{M}|_0 = 118$ for the 27 LCC stars, respectively. As we have shown in the previous section, OB stars entered the LB region 10–15 Myr ago, setting the clock for its origin to $t = 0$. From a further fit to the isochrone data of Schaller et al. (1992) we estimate that the main-sequence lifetime of such bright stars scales with mass as

$$\tau = \tau_0\,\mathcal{M}^{-\alpha} \quad (2\,\mathcal{M}_\odot \leqslant \mathcal{M} \leqslant 67\,\mathcal{M}_\odot) \tag{5}$$

with $\tau_0 = 1.6 \times 10^8$ yr and $\alpha = 0.932$. This means that the masses of the most massive stars $\mathcal{M}_{\Delta\tau}$ in the associations at a look-back time of $\Delta\,\tau$ years ago are given by

$$\mathcal{M}_{\Delta\tau} = \left(\mathcal{M}_\mathrm{u}^{-\alpha} - \frac{\Delta\tau}{\tau_0}\right)^{-1/\alpha}, \tag{6}$$

implying $\mathcal{M}_{10} = 15.4\,\mathcal{M}_\odot$ if $\Delta\tau = 10$ Myr or $\mathcal{M}_{15} = 26.6\,\mathcal{M}_\odot$ if $\Delta\tau = 15$ Myr depending on the entry time of the associations into the volume occupied by the LB today. The expected number of SNe, that is, the number of 'missing' stars, is then calculated by

$$N_\mathrm{SN} = \int_{8.2}^{\mathcal{M}_{\Delta\tau}} \left.\frac{\mathrm{d}N}{\mathrm{d}\mathcal{M}}\right|_0 \mathcal{M}^{-2.1}\,\mathrm{d}\mathcal{M}. \tag{7}$$

We thus obtain estimates of $N_\mathrm{SN} = 8$–12 from the UCL and $N_\mathrm{SN} = 6$–8 from the LCC associations, respectively. The estimate of 14–20 SNe, which created the LB, is in good agreement with the values determined by Maíz-Apellániz (2001) and BB02. Extrapolating the IMF to masses beyond $\mathcal{M}_{\Delta\tau}$ we estimate that 12–5 SNe exploded before the associations entered the present LB volume.

We have noted above that our original sample is complete in radial velocities for stars with colours $(B-V) < -0.1$ which corresponds to $M_V = 0.7$, if an extinction of $A_V = 0.1$ is assumed. According to equation (2) such stars have a mass of $2.95\,\mathcal{M}_\odot$. If we remove 15 stars with colours $(B-V) > -0.1$ from the final sample (79 stars) and modify equation (4) for the cut-off at 2.95 at the low-mass end, we find $\mathrm{d}N/\mathrm{d}\mathcal{M}|_{0,\mathrm{UCL+LCC}} = 291$ instead of 302. Thus the incompleteness of the original sample has not introduced any significant bias in our sample.

In order to assess the question, whether the estimated number of SNe would suffice to excavate the LB, we consider the energy input by the SN explosions into the interstellar gas. According to the IMF (3) there are

$$\mathrm{d}N = \left.\frac{\mathrm{d}N}{\mathrm{d}\mathcal{M}}\right|_0 \mathcal{M}^{\Gamma-1}\,\mathrm{d}\mathcal{M} \tag{8}$$

stars in the mass range $(\mathcal{M}, \mathcal{M} + \mathrm{d}\mathcal{M})$ with main-sequence lifetimes $(\tau, \tau - \mathrm{d}\tau)$. Thus

$$\mathrm{d}N = \left.\frac{\mathrm{d}N}{\mathrm{d}\mathcal{M}}\right|_0 \mathcal{M}^{\Gamma-1}\left(-\frac{\mathrm{d}\mathcal{M}}{\mathrm{d}\tau}\right)\mathrm{d}\tau, \tag{9}$$

and the energy input rate is given by (cf. BB02)

$$\begin{aligned}\dot{\mathcal{E}}_\mathrm{SN} &= \frac{\mathrm{d}}{\mathrm{d}t}\mathcal{E}_\mathrm{SN}N_\mathrm{SN} = \mathcal{E}_\mathrm{SN}\frac{\mathrm{d}N_\mathrm{SN}}{\mathrm{d}t} \\ &= \mathcal{E}_\mathrm{SN}\left.\frac{\mathrm{d}N}{\mathrm{d}\mathcal{M}}\right|_0 \mathcal{M}^{\Gamma-1}(-1)\frac{\mathrm{d}}{\mathrm{d}\tau}\left(\frac{\tau}{\tau_0}\right)^{-1/\alpha}\frac{\mathrm{d}\tau}{\mathrm{d}t},\end{aligned} \tag{10}$$

where $\mathcal{E}_\mathrm{SN}$ denotes the energy released by a single SN, $\mathcal{E}_\mathrm{SN} = 10^{51}$ erg. According to the way we have set up equation (9) $\mathrm{d}\tau/\mathrm{d}t$ is equal to 1. Equation (10) describes the trade-off of the increasing number of SN progenitors and their increasing main-sequence lifetimes with decreasing mass. Inserting the age-to-mass relation (5) into equation (10) leads then to

$$\dot{\mathcal{E}}_\mathrm{SN} = \dot{\mathcal{E}}_\mathrm{SN0}\,t_7^{-(\Gamma+\alpha)/\alpha} \tag{11}$$

with t_7 defined as $t_7 = t/10^7$ yr. For the constant $\dot{\mathcal{E}}_\mathrm{SN0}$ we find

$$\begin{aligned}\dot{\mathcal{E}}_\mathrm{SN0} &= \frac{\mathcal{E}_\mathrm{SN}}{\alpha\tau_0}\left.\frac{\mathrm{d}N}{\mathrm{d}\mathcal{M}}\right|_0 \left(\frac{10^7\ \mathrm{yr}}{\tau_0}\right)^{-0.1803} \\ &= 3.5 \times 10^{35}\left.\frac{\mathrm{d}N}{\mathrm{d}\mathcal{M}}\right|_0 \mathrm{erg\,s^{-1}}.\end{aligned} \tag{12}$$

Equation (11) shows a rather weak decline of the SN energy input rate into the LB as a result of partial compensation between the increasing number of stars with decreasing mass and a corresponding increase in main-sequence lifetime. It is quite remarkable – although probably fortuitous – that the distribution of stellar masses during the star formation process is nearly anticorrelated with the main-sequence lifetime of stars.

BB02 have derived a bubble wind equation which describes the growth of the size of the bubble with time. The radius of the bubble is given by

$$R_\mathrm{b}(t) = R_\mathrm{b0}\,t^{(2\alpha-\Gamma)/5\alpha} \tag{13}$$

with the constant

$$R_{\rm b0} = \left[\frac{475\alpha}{(4\alpha-7\Gamma)(3\alpha-4\Gamma)}\right]^{1/5}\left[\frac{\alpha\dot{\mathcal{E}}_{\rm SN0}\,\tau_0^{1+\Gamma/\alpha}}{2\pi(2-\Gamma)\rho_0}\right]^{1/5}. \quad (14)$$

We note in passing that equations (13) and (14) are consistent with equations (14)–(16) of BB02, except for a different value of α used here, and a normalization error in BB02, where L_0 and ρ_0 should be replaced by $\tilde{L}_0 = L_0/t_0^{\delta}$ with $\delta = -(1+\Gamma/\alpha)$ and $\tilde{\rho}_0 = \rho_0/R_0^{\beta}$. In equation (13) a constant density ρ_0 of the ambient interstellar gas is assumed for which we adopt a value of $\rho_0 = 2\times10^{-24}$ g cm^{-3}. The index in equation (13), $(2\alpha-\Gamma)/5\alpha = 0.564$, lies between the index of 0.4 of the Sedov equation, describing SN remnants, and the index of 0.6 of the stellar wind/superbubble expansion law. For a LB age of 10–15 Myr equation (13) predicts a bubble radius of 78–100 pc, respectively. This is in good agreement with the observed size of the LB in the Galactic disc, as determined by Lallement et al. (2003; cf. also Fig. 7). For the determination of the expected LB size we have used the expected numbers of SNe both from the LCC and UCL subgroups. Maíz-Apellániz (2001) has argued that the LB owes its existence only to the six SNe stemming from the LCC subgroup, because stars from this subgroup came closest to the Sun in the past. We find the same when tracing the orbits of the stars backwards in time. However, the members of the UCL subgroup did enter the region occupied by the LB today and SNe stemming from the UCL subgroup have to be taken into account, in our view, in the energy considerations as well. The energy input of six SNe would excavate a bubble with radius of only 65 pc, which is more difficult to reconcile with the fact that the walls of the LB have been blown out above and below the Galactic plane so that the LB has become effectively a chimney. In general, however, similarity solutions as applied here can only give a rough estimate of the LB age and size due to several severe restrictions. First, the ambient medium has to be assumed to be either homogeneously distributed or to follow a power law distribution in density and its pressure has to be small compared to the bubble pressure. Secondly, turbulent mixing and mass loading, which occur in real bubbles, are hard to incorporate without further assumptions (cf. Dyson, Arthur & Hartquist 2002). Therefore the most realistic approach to model *existing bubbles* is to perform 3D high-resolution numerical simulations of their formation. A first simulation of this kind was carried out by Breitschwerdt & Avillez (2006) which was based on the older and less detailed LB formation scenario of BB02. In the next section, we present an upgrade of that simulation which is now based on the better understood SN rate and the calculated paths of their progenitors through the LB as derived in this paper.

3.3 High-resolution simulations of the LB evolution

We have simulated the effects of the explosions of the stars formerly belonging to the UCL and LCC subgroups as their trajectories have crossed the LB volume towards their present positions. The crucial physical boundary conditions we have to apply to our simulations are the locations, the masses, and derived from this, the explosion times of the SNe responsible for the origin of the LB. The latter can be inferred from equations (8) and (10) to be

$$\frac{{\rm d}N}{{\rm d}\tau} = \frac{1}{\alpha\tau_0}\frac{{\rm d}N}{{\rm d}\mathcal{M}}\bigg|_0\left(\frac{\tau}{\tau_0}\right)^{-(\Gamma+\alpha)/\alpha}, \quad (15)$$

which can be integrated to

$$N(\tau) = \frac{1}{\Gamma}\frac{{\rm d}N}{{\rm d}\mathcal{M}}\bigg|_0\left[\mathcal{M}_{\Delta\tau}^{\Gamma} - \left(\frac{\tau}{\tau_0}\right)^{-\Gamma/\alpha}\right], \quad (16)$$

taking the mass of the most massive star as an upper boundary.

We then proceed, somewhat arbitrarily, to bin the number of exploded stars between $\mathcal{M}_u$ and $\mathcal{M}_{\Delta\tau}$ modulo integer solar masses, and derive their main sequence and hence explosion times from equation (5). Next, the explosion locations are fixed by assuming that the presently 'missing stars' were following the centres of mass of their respective subgroups.

The 3D high-resolution simulations are based on a hydrodynamical Godunov scheme (cf. Godunov & Ryabenki 1964) supplemented by adaptive mesh refinement (AMR) along the lines described by Avillez & Breitschwerdt (2004) and Breitschwerdt & Avillez (2006). This entails a detailed treatment of the evolution of the interstellar gas in a volume of the Galaxy with a square area of 1 kpc^2 and a vertical extent of 10 kpc on either side of the Galactic mid-plane based on the 3D SN-driven ISM model of Avillez (2000) and Avillez & Breitschwerdt (2004). In these calculations the ISM is disturbed by background SN explosions at the Galactic rate. Initial conditions for the *ambient medium* were chosen from a data cube of a previous hydrodynamical run where the highest AMR resolution was 1.25 pc (Avillez & Breitschwerdt 2004; Breitschwerdt & Avillez 2006). As a specific boundary condition we have to include the simultaneous evolution of the Loop I superbubble, which has been observed to interact with the LB according to *ROSAT* PSPC observations (Egger & Aschenbach 1995). We therefore selected a site with enough mass to form all the high-mass stars which are expected to explode as SNe. Using the same IMF for Galactic OB associations we derived in total 81 stars with masses $\mathcal{M}$ between 7 and 31$\mathcal{M}_\odot$ which in our simulations compose the Sco Cen cluster; 39 massive stars with $14 \leqslant \mathcal{M} \leqslant 31\,\mathcal{M}_\odot$ have already gone off, generating the Loop I cavity (see Egger 1998, see also Avillez & Breitschwerdt 2005a). Presently the Sco Cen cluster, which is located at (375, 400) pc in the top panel of Fig. 8, hosts 42 stars to explode within the next 13 Myr. Periodic boundary conditions are applied along the four vertical boundary faces of our computational volume, while outflow boundary conditions are imposed at the top ($z = 10$ kpc) and bottom ($z = -10$ kpc) boundaries. The simulation time of this run was 30 Myr.

Fig. 8 shows the temperature (top) and pressure (bottom) distributions in the Galactic mid-plane 13.4 Myr after the explosion of the first SN, only a few thousand years after the last UCL and LCC SNe with masses of 8.2$\mathcal{M}_\odot$ have exploded. This can be seen as a red spot at $(x, y) = (200, 300)$ pc. The LB is located in the region between $100 \leqslant x \leqslant 300$ pc and $250 \leqslant y \leqslant 550$ pc, its centre being located at $(x, y) = (200, 400)$ pc. The shock waves of the last two SNe occurring within the LB are most noticeable in the P/k distribution by the high-pressure peak shown in the bottom panel. To the right-hand side of the LB the shell of Loop I can be seen, which due to its high temperature will emit in soft X-rays (top panel), consistent with *ROSAT* PSPC observations.

Another striking feature in Fig. 8 (bottom panel) are the coherent bubble structures within a highly disturbed background medium with a pressure in the range $2 \leqslant \log(P/k) \leqslant 4$ which are due to the locally enhanced SN rates in the vicinity of the Sun and in the Loop I region. The successive explosions close to the Sun heat and pressurize the LB, which at first looks smooth, but develops internal temperature and density structures at later stages. About 13.4 Myr after the first explosion the LB cavity, which is bounded by an outer shell will start to fragment due to Rayleigh–Taylor instabilities, in agreement with a linear stability analysis carried out by Breitschwerdt, Egger & Freyberg (2000). It then fills a volume roughly corresponding to the present-day LB size.

A more detailed analysis of these results and their observational consequences will be the subject of forthcoming papers.

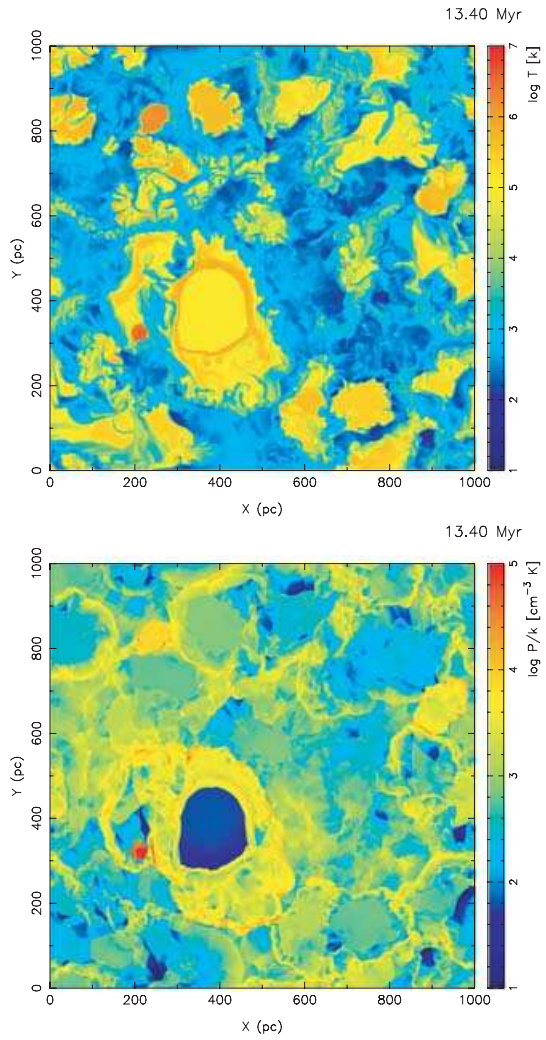

Figure 8. Temperature (top panel) and pressure (bottom panel) distributions in the Galactic mid-plane 13.4 Myr after the first explosion in UCL occurred. The pressure is given in units of cm^{-3} *K*, that is, divided by Boltzmann's constant *k*. The dimensions and morphology of the LB are similar to the present observations. Loop I, to the right-hand side of the LB, is bounded by an X-ray-illuminated shell (top panel).

4 CONCLUSIONS AND OUTLOOK

In contrast to previous analyses of the origin of the LB we have not merely selected presently known stellar subgroups and traced their kinematics back in time. Instead we have scrutinized *ab initio* a large sample volume of stars for stellar groups by analysing their spatial and kinematical properties. From such an unbiased search among nearby B stars we confirm the rather robust result that besides the US subgroup the UCL, and LCC subgroups with ages of 20–30 Myr are the youngest stellar associations in the solar neighbourhood. Our search volume is presently limited to a diameter of 400 pc, because the *Hipparcos* parallaxes are not accurate enough at distances larger than 200 pc. Hence the analysis of a larger volume has to await the launch of GAIA.

Our search strategy relied mainly on kinematical criteria, and we found many other B stars with the same kinematics as the subgroups. We have followed the paths of the associations into the past and find that they entered the region of the present LB 10–15 Myr ago. Deriving O VI column densities from a numerical simulation of the general ISM (Avillez & Breitschwerdt 2005b) as well as of LB and Loop I evolution (Breitschwerdt & Avillez 2006) in a realistic background medium, excellent agreement was found with O VI absorption-line data obtained with FUSE (Oegerle et al. 2005; Savage & Lehner 2006). According to numerical LB evolution simulations by Breitschwerdt & Avillez (2006), who used SNe from the subgroup B1 of the Pleiades to power the LB, the O VI data can be fitted with a LB age of $14.4 \pm \frac{0.7}{0.4}$ Myr. The age of 13.9–14.1 Myr estimated from the present simulation is thus consistent with the age estimated from the slightly different simulation by Breitschwerdt & Avillez (2006). We therefore conclude that the LB must have been excavated during this time. We find that about 14–20 SNe originated from the associations LCC and UCL. The implied energy input into the ambient interstellar gas explains quantitatively the present size of the LB.

The LB serves as an ideal test laboratory for superbubble models due to the wealth of observations against which they can be tested. Apart from the important O VI test, we will also compare EUV and soft X-ray emission data with our models in order to derive the excitation history of ions in the LB and a possible deviation from CIE.

ACKNOWLEDGMENTS

This research has made extensive use of the Simbad data base at CDS, Strasbourg, France. This work has been partially funded by the Portuguese Science Foundation under the project PESO/P/PRO/40149/2000 to MAdeA and DB. CF thanks the Academy of Finland for funding a one-month stay in Germany during which part of this work was carried out. We thank Verena Baumgartner for careful reading of the manuscript.

REFERENCES

Avillez M. A., 2000, MNRAS, 315, 479
Avillez M. A., Breitschwerdt D., 2004, A&A, 425, 899
Avillez M. A., Breitschwerdt D., 2005a, in Chyży K. T., Otmianowska-Mazur K., Soida M., Dettmar R.-J., eds, The Magnetized Plasma in Galaxy Evolution. Jagiellonian University, Kraków, p. 66
Avillez M. A., Breitschwerdt D., 2005b, ApJ, 634, L65
Berghöfer T. W., Breitschwerdt D., 2002, A&A, 390, 299 (BB02)
Bertelli G., Bressan A., Chiosi C., Fagotto F., Nasi E., 1994, A&AS, 106, 275
Blaauw A., 1964, ARA&A, 2, 213
Bochkarev N. G., 1987, ApSS, 138, 229
Breitschwerdt D., 2001, ApSS, 276, 163
Breitschwerdt D., Avillez M. A., 2006, A&A, 452, L1
Breitschwerdt D., Schmutzler T., 1994, Nat, 371, 774
Breitschwerdt D., Freyberg M. J., Trümper J., 1998, eds, IAU Coll. 166, The Local Bubble and Beyond. Springer-Verlag, Berlin, p. 603
Breitschwerdt D., Egger R., Freyberg M. J., 2000, A&A, 361, 303
Cox D. P., Anderson P. R., 1982, ApJ, 253, 268
de Bruijne J. H. J., 1999, MNRAS, 310, 585
de Geus E. J., de Zeeuw P. T., Lub J., 1989, A&A, 216, 44
de Zeeuw P. T., Hoogerwerf R., de Bruijne J. H. J., Brown A. G. A., Blaauw A., 1999, AJ, 117, 354
Dehnen W., Binney J., 1998, MNRAS, 298, 387
Drimmel R., Smart R. L., Lattanzi M. G., 2000, A&A, 354, 67
Dyson J. E., Arthur S. J., Hartquist T. W., 2002, A&A, 390, 1063
ESA, 1997, ESA SP-1200, The Hipparcos and Tycho catalogues. ESA Publications Division, Noordwijk
Egger R., 1998, in Breitschwerdt D., Freyberg M. J., Trümper J., eds, IAU Coll. 166, The Local Bubble and Beyonbd. Springer-Verlag, Berlin, p. 287
Egger R., Aschenbach B., 1995, A&A, 294, L25
Elias F., Alfaro E. J., Cabrera-Caño J., 2006, AJ, 132, 1052

Feast M., Whitelock P., 1997, MNRAS, 291, 683
Freyberg M. J., 1998, in Breitschwerdt D., Freyberg M. J., Trümper J., eds, IAU Coll. 166, The Local Bubble and Beyond. Springer-Verlag, Berlin, p. 113
Frisch P. C., 1995, Space Sci. Rev., 72, 499
Godunov S. K., Ryabenki V. S., 1964, Theory of Difference Schemes – An Introduction. North-Holland, Amsterdam
Holmberg J., Flynn C., 2004, MNRAS, 352, 440
Hoogerwerf R., Aguilar L. A., 1999, MNRAS, 306, 394
Hurwitz M., Sasseen T. P., Sirk M. M., 2005, ApJ, 623, 911
Innes D. E., Hartquist T. W., 1984, MNRAS, 209, 7
Jelinsky P., Vallerga J. V., Edelstein J., 1995, ApJ, 442, 653
Kamaya H., 2004, AJ, 128, 761
Lallement R., 2004, A&A, 422, 391
Lallement R., Welsh B. Y., Vergely J. L., Crifo F., Sfeir D., 2003, A&A, 411, 447
Lindblad B., 1959, Handbuch der Physik, 53, 21
Maeder A., 1981a, A&A, 93, 136
Maeder A., 1981b, A&A, 99, 97
Maeder A., 1981c, A&A, 102, 401
Maíz-Apellániz J., 2001, ApJ, 560, L83
Massey P., Johnson K. E., Degioia-Eastwood K., 1995, ApJ, 454, 151
McCammon D. et al., 2002, ApJ, 576, 188
Mermilliod J. C., Hauck B., Mermilliod M., 1997, A&AS, 124, 349
Oegerle W. R., Jenkins E. B., Shelton R. L., Bowen D. V., Chayer P., 2005, ApJ, 622, 377
Sanders W. T., Edgar R. J., Kraushaar W. L., McCammon D., Morgenthaler J. P., 2001, ApJ, 554, 694
Sartori M. J., Lépine J. R. D., Dias W. S., 2003, A&A, 404, 913
Savage B. D., Lehner N., 2006, ApJS, 162, 134
Schaller G., Schaerer D., Meynet G., Maeder A., 1992, A&AS, 96, 269
Sfeir D. M., Lallement R., Crifo F., Welsh B. Y., 1999, A&A, 346, 785
Smith R. K., Cox D. P., 2001, ApJS, 134, 283
Torra J., Fernández D., Figueras F., 2000, A&A, 359, 82
Wielen R., 1982, in Schaifers K., Voigt H. H., eds., Astronomy and Astrophysics, Vol. 2, XVIII, Landolt-Börnstein: Numerical Data and Functional Relationships in Science and Technology – New Series, Gruppe/Group 6. Springer-Verlag, Berlin, p. 208

APPENDIX A: *HIPPARCOS* NUMBERS OF SELECTED STARS.

Table A1. Identified members of US (ass = 1), UCL (ass = 2) and LCC (ass = 3). Positional and velocity errors are given by the ϵ_i.

HIP-no.	ass	M_V (mag)	$(B-V)_0$ (mag)	X (pc)	Y (pc)	Z (pc)	U (km s^{-1})	V (km s^{-1})	W (km s^{-1})	ϵ_X	ϵ_Y	ϵ_Z	ϵ_U	ϵ_V	ϵ_W
50847[13]	3	−0.63	−0.132	42.7	−123.3	−18.6	−11.06	−16.11	−3.62	2.8	8.1	1.2	1.5	3.5	0.6
53701[15]	3	0.82	−0.098	37.8	−104.6	−2.6	−8.03	−19.46	−5.77	2.5	6.9	0.2	1.6	3.5	0.6
55425[15]	3	−1.07	−0.157	33.4	−92.1	10.4	−10.80	−14.61	−5.61	1.8	4.8	0.6	1.5	3.5	0.6
57851	3	−0.31	−0.156	46.6	−92.5	−5.5	−4.95	−25.11	−8.09	2.7	5.4	0.3	1.2	1.6	0.5
58326	3	−0.73	−0.157	82.6	−163.8	−0.7	−8.65	−26.16	−8.81	7.9	15.6	0.1	2.4	3.4	1.0
58720	3	1.01	−0.080	45.0	−82.5	−11.1	−11.33	−13.92	−7.20	2.3	4.2	0.6	1.9	3.2	0.6
59173	3	−0.94	−0.192	49.4	−101.5	23.2	−7.84	−23.69	−4.98	4.1	8.4	1.9	1.5	1.8	0.9
59449	3	−1.17	−0.171	46.6	−92.2	18.3	−9.60	−23.79	−9.51	3.6	7.1	1.4	2.1	3.4	1.2
59747	3	−2.45	−0.237	52.7	−98.1	7.4	−5.49	−28.71	−6.86	3.5	6.6	0.5	1.4	1.7	0.6
60009	3	−1.20	−0.187	54.2	−96.5	−2.6	−6.81	−21.74	−8.00	3.3	5.9	0.2	1.0	0.8	0.6
60710	3	−0.68	−0.162	58.2	−105.2	23.9	−12.13	−13.98	−6.34	4.9	8.9	2.0	2.2	3.3	1.0
60823	3	−1.76	−0.198	64.5	−115.9	29.3	−12.72	−18.47	−7.94	5.9	10.6	2.7	2.3	3.3	1.3
61585	3	−2.17	−0.212	48.9	−79.3	−10.3	−8.39	−19.51	−7.89	2.2	3.6	0.5	2.0	3.2	0.5
62058	3	0.47	−0.079	66.4	−107.2	14.8	−9.90	−19.18	−6.21	5.4	8.7	1.2	1.5	1.7	0.7
62327	3	−0.86	−0.183	64.3	−102.0	13.5	−6.65	−24.85	−6.89	4.7	7.4	1.0	1.5	1.7	0.7
62434[16]	3	−3.92	−0.240	57.9	−91.1	6.0	−12.21	−26.68	−6.05	3.8	6.0	0.4	1.5	1.1	0.6
63003	3	−1.29	−0.180	63.3	−96.2	11.5	−6.03	−21.39	−5.81	4.2	6.5	0.8	1.0	0.9	0.6
63005	3	−0.29	−0.148	60.6	−92.0	11.0	−6.83	−20.64	−4.21	4.1	6.2	0.7	2.2	3.2	0.6
63007	3	−0.63	−0.166	60.5	−92.0	7.2	−7.81	−20.05	−6.70	4.0	6.1	0.5	2.2	3.2	0.6
63945	3	−0.83	−0.147	71.3	−100.1	31.4	−10.48	−16.96	−6.03	6.5	9.1	2.9	2.4	3.1	1.2
64004[13]	3	−1.35	−0.227	71.5	−100.2	28.2	−4.21	−21.89	−3.11	7.3	10.2	2.9	2.5	3.1	1.1
64053	3	0.64	−0.093	56.8	−80.0	16.1	−1.27	−29.22	−4.81	3.7	5.2	1.0	2.3	3.1	0.9
64425[18]	3	−0.56	−0.081	61.6	−86.3	5.3	−5.04	−18.79	−6.99	9.9	13.9	0.9	2.9	3.4	1.4
65112	3	0.05	−0.132	72.6	−95.0	20.8	−8.05	−20.15	−5.56	5.9	7.7	1.7	2.5	3.1	0.9
65271	3	−0.78	−0.173	64.9	−87.1	3.1	−11.63	−16.36	−5.38	4.1	5.5	0.2	2.4	3.1	0.4
66454	3	0.52	−0.112	75.7	−86.6	32.4	−7.46	−17.85	−3.78	6.9	7.9	2.9	2.3	2.6	1.1
67036[03]	3	1.18	0.098	73.0	−83.0	21.5	−6.08	−19.46	−5.23	6.2	7.0	1.8	1.5	1.7	0.8
67464[13]	2	−2.40	−0.229	95.8	−97.8	49.5	−7.33	−22.19	−6.12	10.7	11.0	5.6	1.5	2.0	1.1
67472[05]	2	−2.58	−0.180	106.5	−109.4	52.9	−6.86	−23.38	−6.42	12.2	12.5	6.1	2.4	2.7	1.4
67669	2	−0.54	−0.149	59.1	−54.6	43.1	−4.63	−20.69	−3.96	4.7	4.4	3.5	1.3	1.6	1.1
67973	2	0.51	−0.090	70.2	−75.9	17.3	−0.22	−24.56	−3.88	4.8	5.2	1.2	3.4	3.7	1.0
68245	2	−1.94	−0.219	96.9	−93.7	46.6	−7.62	−19.12	−6.37	9.3	9.0	4.5	1.5	1.8	1.0
68282	2	−1.68	−0.209	87.3	−86.4	36.3	−9.09	−18.99	−6.43	7.8	7.7	3.2	1.6	1.8	0.9
68862	2	−1.33	−0.199	95.4	−86.7	45.8	−4.18	−22.32	−4.88	9.8	8.9	4.7	2.3	2.5	1.4
69618[06]	2	−1.07	−0.138	103.5	−106.7	10.3	−9.63	−19.90	−8.16	9.1	9.4	0.9	5.3	5.5	1.0
70300	2	−1.16	−0.199	94.5	−75.0	44.0	−7.24	−18.06	−5.30	9.2	7.3	4.3	1.5	1.8	0.8

Table A1 – *continued*

HIP-no.	ass	M_V (mag)	$(B-V)_0$ (mag)	X (pc)	Y (pc)	Z (pc)	U (km s^{-1})	V (km s^{-1})	W (km s^{-1})	ϵ_X	ϵ_Y	ϵ_Z	ϵ_U	ϵ_V	ϵ_W
70455	2	0.92	−0.089	115.1	−91.9	50.0	−1.80	−24.44	−3.46	15.4	12.3	6.7	4.7	4.2	2.2
70626	2	0.62	−0.087	104.6	−81.3	46.7	−3.76	−19.72	−6.36	11.6	9.0	5.2	2.1	2.4	1.4
71352[07]	2	−2.73	−0.270	72.2	−54.8	27.1	−10.77	−17.42	−6.55	5.7	4.3	2.1	1.5	1.7	0.8
71453	2	0.19	−0.117	98.5	−72.0	40.5	−7.53	−16.98	−5.52	9.8	7.1	4.0	3.0	2.6	1.4
71536[03]	2	−0.84	−0.150	72.0	−60.1	16.3	−3.79	−18.67	−5.44	4.9	4.1	1.1	5.6	4.8	1.4
71724[15]	2	1.16	−0.086	94.9	−68.5	36.9	−5.83	−15.03	−6.25	9.7	7.0	3.8	1.1	1.6	1.0
71727[15]	2	0.57	−0.124	123.7	−96.5	36.2	−9.74	−20.50	−8.01	16.9	13.2	5.0	5.9	5.1	2.2
71860[09]	2	−3.87	−0.222	129.1	−102.3	33.3	−8.77	−22.92	−9.13	16.5	13.1	4.3	1.7	2.5	1.6
71865	2	−0.88	−0.187	72.7	−49.2	32.1	−6.09	−17.31	−5.17	4.9	3.3	2.2	1.2	1.3	0.7
72683[10]	2	−1.21	−0.167	99.2	−69.7	30.5	−4.44	−21.75	−5.35	9.7	6.8	3.0	1.1	1.7	0.8
72800	2	−0.34	−0.167	94.3	−59.1	38.6	−2.09	−16.26	−1.16	8.4	5.3	3.5	1.6	1.5	0.7
73334	2	−2.99	−0.216	133.9	−87.4	42.1	−2.94	−22.31	−5.53	16.1	10.5	5.1	1.3	2.1	1.0
73807[15]	2	−2.01	−0.186	123.5	−85.4	26.3	−8.33	−21.29	−3.97	18.1	12.5	3.8	3.5	3.4	1.2
74066[15]	2	0.24	−0.150	104.9	−62.6	33.2	−8.53	−23.00	−5.73	11.3	6.7	3.6	6.2	4.3	2.1
74100	2	0.18	−0.118	112.5	−70.2	31.1	−7.15	−17.28	−4.37	12.6	7.8	3.5	3.4	2.7	1.3
74479[15]	2	0.83	−0.091	93.5	−48.6	35.3	−8.96	−14.13	−4.21	8.6	4.5	3.2	3.2	2.2	1.3
74950[11]	2	−0.40	−0.103	133.7	−74.6	38.0	0.26	−24.24	−2.81	15.2	8.5	4.3	6.3	4.1	2.0
75141[13]	2	−2.79	−0.238	133.3	−72.9	37.4	−11.02	−18.73	−7.28	17.9	9.8	5.0	2.7	3.0	1.2
75151[15]	2	1.11	−0.113	105.6	−54.4	33.6	−8.85	−13.54	−5.13	14.6	7.5	4.7	5.5	3.4	1.9
75264	2	−2.61	−0.192	130.6	−77.8	27.7	−3.20	−21.98	−2.56	12.3	7.3	2.6	3.3	2.6	0.9
75304	2	−1.83	−0.158	159.8	−78.5	53.6	−8.17	−22.61	−5.98	22.9	11.2	7.7	2.7	3.5	1.3
75647	2	−0.08	−0.148	111.3	−52.8	36.1	−7.74	−17.37	−4.39	12.0	5.7	3.9	8.7	4.6	2.9
76297	2	−3.41	−0.217	151.9	−76.7	35.8	−8.26	−21.78	−8.70	32.8	16.5	7.7	8.9	6.4	2.9
76371	2	−1.07	−0.184	115.1	−63.8	20.3	−2.86	−19.47	−2.27	11.2	6.2	2.0	1.7	1.8	0.6
76395	2	0.95	−0.103	99.4	−39.3	35.1	−8.24	−14.60	−4.54	9.3	3.7	3.3	3.3	2.0	1.3
76945	2	−0.67	−0.145	108.5	−42.8	33.6	−3.21	−22.09	−3.65	11.1	4.4	3.4	1.7	2.2	1.0
77286	2	0.23	−0.118	107.2	−40.8	32.0	−0.87	−19.16	−2.89	11.6	4.4	3.5	6.7	3.2	2.1
77635	1	−1.77	−0.170	144.3	−35.7	59.2	−5.12	−19.74	−7.55	21.0	5.2	8.6	4.3	3.0	2.0
77840[01]	1	−1.31	−0.160	120.4	−28.1	49.0	−10.45	−15.61	−8.52	18.9	4.4	7.7	1.5	2.6	1.1
77900	1	−0.01	−0.096	148.2	−38.1	55.7	−3.92	−21.17	−7.88	19.5	5.0	7.3	2.4	3.0	1.3
77909	1	0.04	−0.097	126.7	−29.0	51.2	−9.40	−15.78	−9.41	21.2	4.8	8.6	3.4	2.8	1.6
78207[02]	1	−1.03	−0.089	137.7	−8.7	75.3	−6.74	−15.01	−5.07	17.1	1.1	9.4	1.6	2.0	1.0
78246[13]	1	−0.60	−0.140	136.6	−28.7	54.1	−12.34	−15.49	−10.56	16.8	3.5	6.6	3.1	2.2	1.5
78265[13]	1	−2.85	−0.249	128.9	−29.2	48.7	−12.31	−15.32	−10.47	15.2	3.5	5.8	6.8	2.6	2.7
78384	2	−2.48	−0.226	138.4	−53.8	28.9	−5.80	−21.12	−6.28	16.3	6.3	3.4	3.6	2.8	1.2
78655	2	−1.14	−0.141	148.4	−56.6	29.2	−9.36	−22.89	−7.30	18.2	6.9	3.6	2.8	3.0	1.1
78756[15]	2	0.83	−0.056	153.9	−59.9	28.0	−6.36	−22.90	−4.40	24.5	9.5	4.5	6.9	4.5	1.7
78877[04]	1	−0.02	−0.096	137.5	−23.4	53.1	−6.35	−19.40	−10.64	17.6	3.0	6.8	3.4	2.7	1.7
79044	2	1.15	−0.077	120.5	−40.4	25.9	−2.31	−20.04	−5.47	12.5	4.2	2.7	6.9	3.0	1.7
79404	1	−1.32	−0.197	134.4	−28.3	41.6	−5.18	−15.43	−6.86	15.2	3.2	4.7	6.9	2.4	2.3
81914	2	0.15	−0.119	141.9	−44.0	8.1	−6.73	−14.66	−3.91	18.0	5.6	1.0	1.8	2.0	0.6
82545	2	−2.47	−0.223	153.6	−37.7	10.7	−3.26	−19.78	−3.70	20.9	5.1	1.5	0.9	2.7	0.8
84970	1	−2.95	−0.223	171.6	1.4	19.7	−1.37	−20.10	−5.05	20.5	0.2	2.3	3.6	2.3	1.0

[1]multiple, [2]emm.l./variable, [3]variable, [4]rotnl. variable, [5]Be, [6]emm.l./binary, [7]Be/neb.emm., [9]variable/βCep, [10]binary, [11]ecl.binary, [12]variable/βCep, [13]spec.binary, [15]double, [16]variable/βCep/double?, [18]ellips.variable/double?

Table A2. HIP-nos. of the remaining selected stars.

2484	2505	5566	7588	7943	8886	10602	10944	11249	12692
15338	15404	15444	15627	15770	15988	16147	16210	16244	16470
16611	16803	17499	17531	17563	17573	18033	18190	18213	18216
18788	19860	20042	20063	20171	20186	20884	21192	21281	22109
23607	23767	24244	25813	26248	26487	26623	26640	29426	30069
30122	30675	31278	31362	31685	32677	32912	33015	33579	34045
35054	35785	36188	37304	38455	38863	39138	39360	39906	40581
42177	42637	43105	43394	43878	43937	45080	45418	45941	46283
47119	47391	47452	51437	51576	52370	52419	52502	52701	52736
54767	55597	58484	60000	60718	60855	61789	62786	65474	66821
67301	68269	69389	71353	76243	76669	78493	79653	82673	82902
83895	85391	85792	86414	89482	89908	90200	90422	91235	91729
92614	92855	93104	93187	93231	93299	93805	95400	95951	96052
96417	96468	97376	98412	98754	100751	101017	101421	101475	101716
101746	101868	103089	103532	103616	104105	105148	105282	106604	107462
107664	107930	108022	109139	112781	115990	116805			

This paper has been typeset from a TEX/LATEX file prepared by the author.